Growth, interfacial microstructure and optical properties of NiO thin films with various types of texture

Y. Wang, J. Ghanbaja, P. Boulet, D. Horwat, J.F. Pierson

Growth, interfacial microstructure and optical properties of NiO thin films with various types of texture

Y. Wang[1,2], J. Ghanbaja[2], P. Boulet[2], D. Horwat[2], J.F. Pierson[2,*]

[1] State Key Laboratory for Environmental-friendly Energy Materials, Southwest University of Science and Technology, Mianyang 621010, China.

[2] Institut Jean Lamour, UMR 7198-CNRS, Université de Lorraine, Nancy F-54011, France.

* corresponding author's e-mail: jean-francois.pierson@univ-lorraine.fr

Abstract

NiO thin films with random, fiber and in-plane textures have been successfully deposited at near room temperature by reactive magnetron sputtering on glass, silicon and Al_2O_3 (0001) substrates. Self-texture related with the deposition conditions and crystallographic characters competes with the driving force from the matched substrate. Such a competition can be used to control the texture of thin films on matched substrates, especially when the promoting orientations from self-texture and substrate are different. Enhancing this competition tends to suppress the self-texture of NiO thin films on Al_2O_3 (0001) substrates, whereas restricting the competition is beneficial to produce the in-plane textured NiO thin films. In addition, it is found that the optical transmittance of NiO thin films on Al_2O_3 (0001) substrates can also be tuned by such competition. Interfacial microstructure analyses of NiO thin films on amorphous substrates clearly evidence the existence a nanocomposite layer at the initial growth, which is composed of NiO nanocrystals surrounded by amorphous matrix. In contrast, in-plane textured NiO thin films on Al_2O_3 (0001) substrates exhibit sharp interface without nanocrystals or amorphous matrix. We believe these results provide a general framework of tuning the textures and properties of thin films on matched substrates.

Keywords: Reactive sputtering; Texture; Thin films; Interfacial microstructure

1. Introduction

Texture, which describes the statistical distribution of grain orientations, is an important microstructural characteristic of thin films, as it can strongly influence the various functional properties [1–10]. Four types of texture component have been identified in thin films: random texture, in which the orientations of grains are fully random (no preferred growth orientation); fiber texture [1,11,12], where the orientation of a lattice plane is preferentially parallel to the substrate plane, while there is some rotational degree of freedom around the axis perpendicular to the substrate plane; in-plane texture (epitaxy)**,** in which all three axes of the grains in thin film are aligned and fixed by the crystallographic orientations of single crystal substrates [1,11,13,14]; off-normal fiber-like texture (axiotaxy), where the preferred alignment of planes across the interface manifests itself as a fiber texture lying off-normal to the sample surface, with the fiber axis perpendicular to certain planes in the substrate [1,11].

Controlling the texture of sputtered thin films is always full of interest, as sputtering is regarded as a highly versatile manufacturing process associated with relatively low cost and easy fabrication of large-area devices. Most of the sputtered thin films exhibit a fiber texture, even when deposited on amorphous substrates [5,8,12,15,16], and the mechanism behind this fiber texture remains complex due to the out of equilibrium state of the sputtering process [16,17]. This fiber texture can be called as self-texture [2], as the driving force for the formation of texture mainly comes from the deposition conditions and crystallographic characters, rather than from the substrate. However, sometimes the preferred orientation of self-texture is not the expected one, or random texture provides better performances. Therefore, growing thin films with various types of texture is desirable to fulfill different applications. Taking NiO as an example, it crystallizes in the stable phase of cubic rocksalt structure (space group $Fm\bar{3}m$).

Along the <111> crystallographic orientation, NiO is composed of alternative Ni^{2+} and O^{2-} planes with Ni^{2+} or O^{2-} as terminations, giving rise to a net surface charge and an electric dipole moment. This means that it is much more difficult to grow NiO thin films with strong <111> texture, even the polar NiO {111} surfaces with larger work function are attractive for hole transportation in organic solar cells [18]. In the case of resistive random access memory application, poor crystallization without preferred orientation may facilitate the defect movements [19,20], indicating that NiO thin films with random texture are probably favorable. On the contrary, to fabricate high quality p-n junction assembled with n-type ZnO thin films, epitaxial NiO thin films is expected to reduce the interfacial states and then to enhance the electrical performances [21,22].

In this work, NiO thin films with random, fiber and in-plane textures have been successfully deposited at near room temperature by reactive sputtering. The total sputtering pressure, oxygen flow rate and the nature of substrates have been employed to tune the texture. The influence of texture on the microstructure at film-substrate interface and optical properties of thin films have been investigated.

2. Experimental

NiO thin films were deposited on glass (microscopy slides), Si (100) and Al_2O_3 (0001) substrates by reactive pulsed-DC magnetron sputtering in various Ar-O_2 reactive mixtures. No intentional heating was applied to the substrate holder and the self-established deposition temperature was close to room temperature. The argon flow rate was fixed at 25 sccm, while the oxygen one varied in the 3 − 11 sccm range. Thin films were deposited at two total sputtering pressures (0.5 and 1 Pa) by changing the pumping speed via a throttle valve. A pulsed-DC supply (Pinnacle+

Advanced Energy) was connected to the metallic nickel target (2 in. diameter and 1 mm thick with a purity of 99.995%). The current applied to the target, the frequency and the off-time were fixed to 0.3 A, 50 kHz and 4 µs, respectively. The distance between the substrate and the target was fixed at 75 mm. Within these deposition conditions, the metallic nickel target is working in the so-called Compound Sputtering Mode (CSM) where the target surface is oxidized. To clearly evidence the effect of the substrate nature on the film texture, the 3 kinds of substrates (glass, Si and Al_2O_3) were systematically introduced in the chamber in the same deposition run.

X-ray diffraction (XRD, Brucker D8 Advance with Cu $K_{\alpha 1}$ radiation (λ = 0.15406 nm) in Bragg Brentano configuration) was used to investigate the phase structure and the growth orientation of films. Pole figure and Phi (ϕ) scan of NiO thin films were obtained using a Brucker D8 Discover diffractometer (Co Kα radiation, λ = 0.17912 nm). It is worth noting that we have shown that the phase structure, preferred orientation and microstructure of thin films are independent of the nature of non-matched substrate (glass or silicon) in our previous studies, as the native amorphous SiO_2 layer on single crystal Si (100) substrate was not removed [8,12]. Transmission electron microscopy (TEM) investigation for the microstructure was performed by a JEOL ARM 200-Cold FEG equipped with a GIF Quantum ER. For this purpose, the cross-section TEM samples of films deposited on silicon substrates were prepared using a focused ion beam (FIB)-scanning electron microscope (SEM) dual beam system (FEI Helios 600) using the 'in situ' lift-out technique. Final thinning was done with low voltage milling (5 kV) to reduce any possible preparation artifact. The optical transmission spectra were measured using an UV-Vis-NIR spectrometer (Varian Cary 5000). The curvature of a coated silicon substrate has been used to estimate the film stress using the Stoney's formula.

3. Results and discussion

3.1. Tuning the texture of NiO thin films

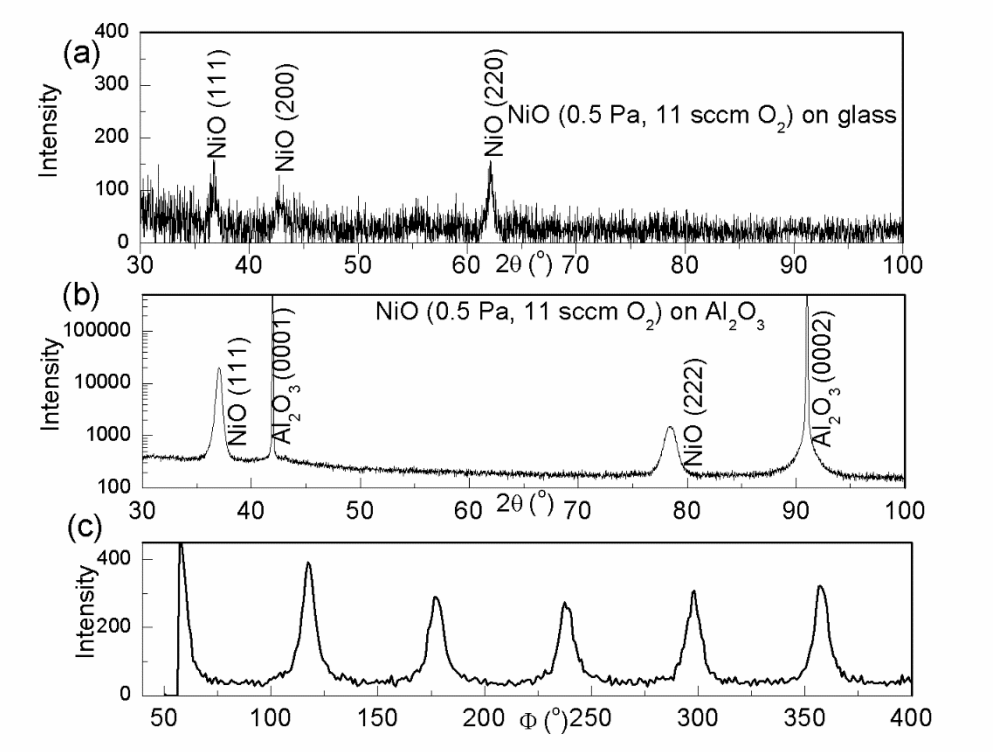

Fig. 1 θ–2θ scan diffractograms of NiO thin films (about 200 nm-thick) deposited on glass (a) and Al_2O_3 (0001) (b) substrates. The oxygen flow rate of 11 sccm O_2 and total sputtering pressure of 0.5 Pa were used. (c) ϕ scan diffractogram of NiO (220) plane (ψ = 35.2°) of NiO thin film on Al_2O_3 (0001) substrate.

First of all, NiO thin films have been grown on glass and Al_2O_3 (0001) substrates in the same deposition run using the following conditions: 0.5 Pa for the total sputtering pressure and 11 sccm for the oxygen flow rate. Fig. 1(a) and (b) show the X-ray θ–2θ scan diffractograms of NiO thin films on glass and Al_2O_3 (0001) substrates, respectively. As seen in Fig. 1(a), the diffractogram of NiO thin film on glass exhibits a very weak signal to background noise ratio, demonstrating the poor crystallization. In addition, the degree of preferred orientation was estimated quantitatively by calculating Harris texture coefficient (T_c), following subtraction of background. T_c is defined as [9,23,24]:

$$T_c(hkl) = n\frac{I_m(hkl)/I_o(hkl)}{\sum_1^n I_m(hkl)/I_o(hkl)} \quad (1)$$

where $I_m(hkl)$ is the measured relative intensity of the diffraction peak belonging to (*hkl*) plane, $I_o(hkl)$ is the relative intensity from the same diffraction plane in the standard powder reference sample, *n* is the total number of diffraction peaks selected for the evaluation. T_c ranges from 0 to *n*. If $T_c(hkl)$ is ~ *n*, the sample exhibits the highly preferred <*hkl*> orientation. On the contrary, samples possess random orientation when $T_c(hkl)$ is ~ 1. In this work, three diffraction peaks ((111), (200) and (220)) of NiO thin films, and standard pattern (JCPDS 00-047-1049) [25] are chosen to calculate T_c, giving the T_c (111), (200) and (220) of 0.94, 0.45, and 1.56 for thin films on glass substrates. These low values associated with the low intensity of the diffraction peaks indicate the random texture of NiO thin films on glass substrates deposited with an oxygen flow rate of 11 sccm and a total sputtering pressure of 0.5 Pa. The magnitude of internal stress was determined by the Stoney's equation; the random textured NiO thin films exhibit the compressive stress of 2.2 $\pm$ 0.3 GPa.

In the case of NiO film deposited on Al_2O_3 (0001) substrate (see Fig. 1(b)), only intense (111) and (222) diffraction peaks of NiO are clearly observed and other out-of-plane orientations are absent. Such a result is in well agreement with previous works related to the deposition of NiO thin films on sapphire substrates [26-29]. T_c(111) of such NiO thin film is 3, indicating that NiO thin film on Al_2O_3(0001) exhibits highly <111> preferred orientation along the out-of-plane direction. In order to investigate the in-plane orientation of such NiO thin film, ϕ scan has been performed. The ϕ scan diffractogram of NiO (220) (ψ = 35.2^o) plane exhibits six sharp peaks with rotational intervals of 60^o (see Fig. 1(c)), demonstrating the growth of epitaxial NiO thin films on Al_2O_3 (0001) substrates. However, six diffraction peaks in Fig. 1(c) is double than the theoretical number of three peaks, which is due to the coexistence of two single-crystal domains with 60^o rotations around [111] axis [26]. This could be understood from both crystallographic characters and the stress behavior. In the viewpoint of crystallographic characters, NiO (111) planes condense along the three-fold-symmetry rhombohedral Al_2O_3 (0001). However, the lattice mismatch is as high as $23.9\% = (\sqrt{2}a_{NiO} - a_{Al_2O_3})/a_{Al_2O_3} * 100$ ($a_{NiO} = 0.417$ nm and $a_{Al_2O_3} = 0.4758$ nm are the crystal constants of NiO and Al_2O_3, respectively). Thus, NiO could hardly grow on Al_2O_3 in this form. By introducing another kind

of domains with 60° rotation [26], the mismatch can be reduced to 7.3% = $(\sqrt{2}a_{NiO} \times 2 - a_{Al_2O_3} \times 2)/(a_{Al_2O_3} \times 2) * 100$, which may facilitate the growth of NiO (111) planes on Al_2O_3 (0001). We tried to estimate the out-of-plane stress of this epitaxial NiO thin film using the formula of $\sigma = \frac{\Delta d}{d} E$, where σ is the strain component along the crystallographic direction, d is the (111) interplanar distance of the standard sample, Δd is the crystal plane difference between our epitaxial thin film and standard sample, and E is the elastic Young's modulus of 95.9 GPa [30]. This gives the out-of-plane compressive stress of about 0.67 GPa, much smaller than the isotropic stress of 2.2 GPa in random textured NiO thin films, even they are deposited at the same time. This also indicates that the epitaxial NiO thin films on Al_2O_3 (0001) substrates possess the anisotropic stress, and the in-plane stress should be much larger than 2.2 GPa. Consequently, the domains can be generated to relax such a high in-plane stress.

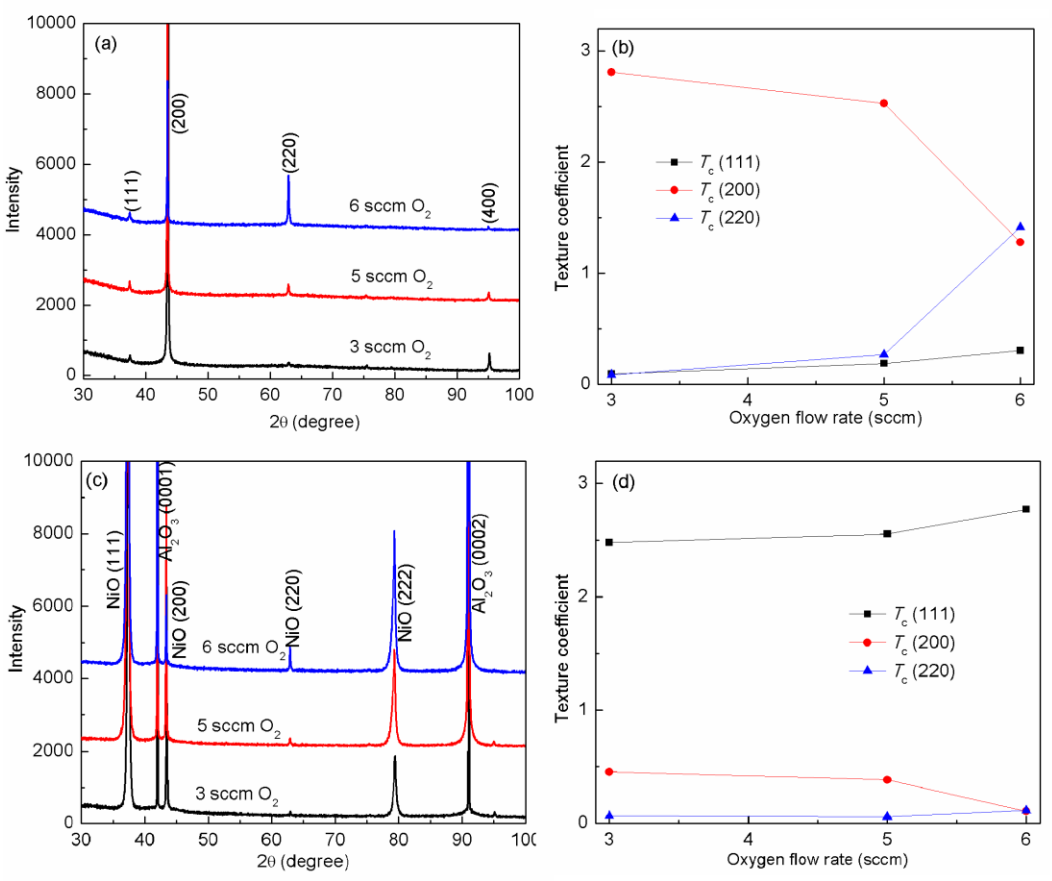

Fig. 2 (a) θ–2θ scan diffractograms and (b) variation of texture coefficient for (111), (200) and (220) diffractions of NiO thin films deposited on glass substrates. (c) θ–2θ scan diffractograms

and (d) variation of texture coefficient for (111), (200) and (220) diffractions of NiO thin films deposited on Al_2O_3(0001) substrates. The total sputtering pressure of 1 Pa and various oxygen flow rates (3, 5 and 6 sccm) have been used to grow these thin films. Thickness is in the range of $320 - 460$ nm. Thin films were deposited on glass and Al_2O_3 (0001) substrates simultaneously.

Changing the total sputtering pressure to 1 Pa, NiO thin films have also been deposited on glass and Al_2O_3 (0001) substrates, simultaneously. Various oxygen flow rates (3, 5 and 6 sccm) have been used to grow NiO thin films. Fig. 2(a) shows the θ–2θ scan diffractograms of these NiO thin film deposited on glass substrate. These diffractograms exhibit more intense (200) diffraction peak than for (111) and (220) planes, indicating the highly <100> preferred orientation along the out-of-plane direction. Taking the NiO thin film deposited with 3 sccm O_2 as an example, pole figures of (200), (111) and (220) planes (see Fig. S1 in the supporting information) evidence that the NiO thin films on glass substrate present a strong fiber texture along <100> orientation. The compressive stress of such fiber textured NiO thin film is about 0.3 $\pm$ 0.1 GPa, which is much lower than that of non-textured thin film. Comparing such fiber textured NiO thin films with non-textured thin films shown in Fig. 1(a), it shows that the total sputtering pressure seems to be an effective approach to tune the texture of NiO thin films on amorphous substrates, accompanying with the change of stress. Thin films deposited at low total pressure (0.5 Pa in the present work) and high oxygen flow rate (11 sccm) may suffer from stronger ions bombardments, especially for ions with negative charge, which will damage the crystallization and texture, yielding random textured thin films with high stress [12,31]. On the contrary, at high pressure the mean free path of the sputtered atoms is lowered, inducing more collisions in the gas phase. This effect decreases the energy of the condensing atoms and lowers the ion bombardment of the growing film. Thus, the use of a high total pressure (1 Pa in the present work) enhances the growth of fiber textured thin films with low intrinsic stress.

With the increase of oxygen flow rate from 3 to 6 sccm, the intensity of (220) diffraction peaks is strongly enhanced (see Fig. 2(a)). The Harris texture coefficient T_c (for (111), (200) and (220) diffraction peaks) is plotted in Fig. 2(b) as a function of the oxygen flow rate. It is shown that T_c (200) falls down significantly from 2.81 to 1.28, whereas T_c (220) rises up from 0.09 to 1.42, with the increase of the oxygen flow rate from 3 to 6 sccm. Such a result implies that high

oxygen flow rate values are detrimental to the fiber texture of NiO thin films on glass substrates with the total sputtering pressure of 1 Pa.

Concerning the NiO thin films grown on Al_2O_3 (0001) substrates with the total sputtering pressure of 1 Pa, (111), (200) and (220) diffraction peaks are clearly observed in all thin films simultaneously (see Fig. 2(c)). This implies the non-epitaxial growth when depositing thin films at the total sputtering pressure of 1 Pa, which is quite different from that of NiO thin films deposited at the total sputtering pressure of 0.5 Pa (see Fig. 1(b) and (c)). Moreover, the evolution of T_c (for (111), (200) and (220) diffraction peaks) as a function of oxygen flow rate is depicted in Fig. 2(d). Since the matched Al_2O_3 (0001) substrate provides a strong driving force, all the NiO films deposited on Al_2O_3 substrate show the highly <111> preferred orientation. However, the T_c (111) increases from 2.48 (3 sccm O_2) to 2.78 (6 sccm O_2) continuously, demonstrating that larger oxygen flow rate is favorable to produce the higher fiber texture for NiO thin films on Al_2O_3 (0001) substrates. Obviously, such tendency is opposite to that of NiO thin films on glass substrates, even deposited at the same time.

Comparing the in-plane and fiber textured NiO thin films in Fig. 1(b) and Fig. 2(c), respectively, it is speculated that both the self-texture and substrate have strong influence on the growth characteristics of thin films on matched single crystal substrates. In NiO, {100} planes usually have the lowest surface energy, giving rise to the high probability to form <100> preferred orientation. Such effect explains that highly <100> fiber textured NiO thin films are easily attained on glass substrates using the total pressure of 1 Pa (see Fig. 2(a)). However, it is much more difficult to produce polar <111> preferred orientation without the use of special substrates (Al_2O_3 (0001) and YSZ (111)). Therefore, there is strong competition between the self-texture and the substrate driving forces when depositing NiO thin films on Al_2O_3 (0001) substrates, which may eventually rearrange the orientation and microstructure of thin films. When the driving force for self-texture is quite weak (like in the case of random texture of NiO thin film on glass substrate deposited at 0.5 Pa shown in Fig. 1(a)), the driving force from Al_2O_3 (0001) substrate may overcome the trend of the self-texture easily. Consequently, the growth behavior is dominated by the substrate, yielding the epitaxial NiO thin films (see Fig. 1(b) and (c)). On the contrary, once the self-texture exhibits certain kind of fiber texture and the preferred orientation is different from that of the substrate, such as NiO thin film deposited at 1 Pa (see Fig. 2(a) and

(c)), the strong competition will result in non-epitaxial NiO thin films with various orientations driven by both self-texture and substrate orientation. In addition, when comparing the texture coefficients of NiO thin films on glass and Al_2O_3 (0001) substrates (see Fig. 2(b) and (d)), it is seen that poorer self-texture within the conditions of high oxygen flow rate (6 sccm) tends to produce much stronger <111> preferred orientation for NiO thin films on Al_2O_3(0001) substrates. This also strongly supports our conclusion that the film microstructure results from the competition between driving forces for the self-texture and for the epitaxy with the substrate. These results provide some practical guidelines to tune the texture of thin films on matched substrates when the promoting orientations from self-texture and substrate are different: (a) Suppressing the self-texture is required to form the epitaxial or highly fiber textured thin films; (b) Enhancing the competition between self-texture and substrate driving force facilitates to reduce or change the fiber texture.

3.2. Microstructure at the film/substrate interface

The microstructure at film-substrate interface region of NiO thin films on Si (100) and Al_2O_3 (0001) substrates has been studied by high resolution TEM (HRTEM). Fig. 3(a) shows the HRTEM image of NiO thin film with random texture on Si (100) substrate (the XRD diffractogram obtained is quite similar with that obtained on glass substrate). Surprisingly, a nanocomposite layer with the thickness of about $6-7$ nm, marked by the red lines in Fig. 3(a), is clearly evidenced between the native amorphous SiO_2 layer and the dense NiO thin film layer. It consists of nanocrystals with a diameter of approx. 4 nm (highlighted by the red ellipse in Fig. 3(a)) embedded in an amorphous matrix. The HRTEM image for the nanocrystals exhibit the crystal planes of NiO with the *d* (200) of about 0.2 nm, as shown in Fig. 3(b). In addition, the energy filtered TEM (EFTEM) mapping is used to check the elemental distribution at this interface region. Fig. 3 (c) is the color mixture image of Ni $L_{3,2}$ edge (in red) and O *K* edge (in green) EFTEM mappings. As seen in Fig. 3(c), the oxygen concentration inside the nanocrystals is smaller than that of the surrounding amorphous thin layers. Besides, the Ni element was detected inside the native amorphous SiO_2 layer, indicating that Ni atoms have diffused or been implanted into the amorphous SiO_2 layer at the initial growth.

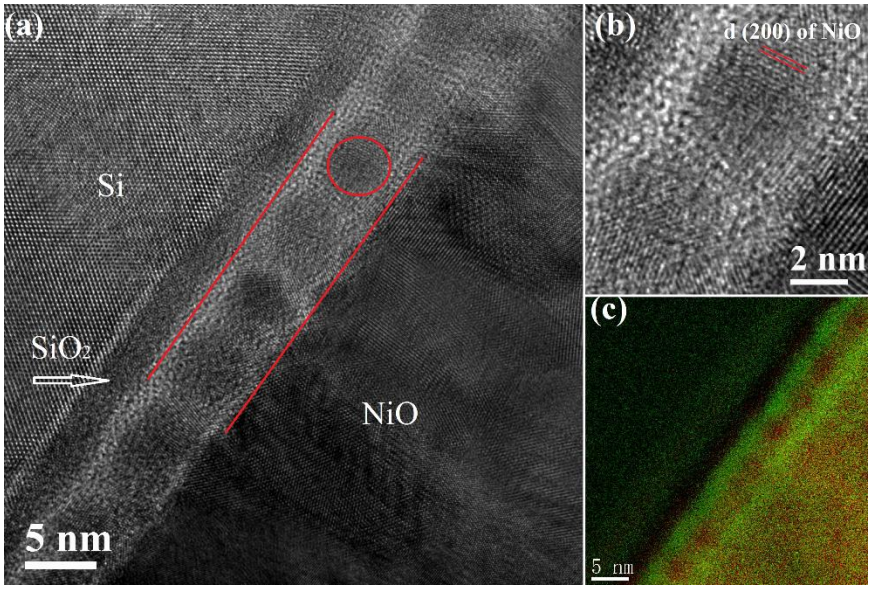

Fig. 3 (a) HRTEM image of NiO thin film with random texture on Si (100) substrate. The native SiO_2 layer on the top of Si(100) is guided by the white arrow. (b) HRTEM image of nanocrystals. (c) Color mixture image of Ni $L_{3,2}$ edge (in red) and O *K* edge (in green) EFTEM mappings.

The interfacial microstructure of epitaxial NiO thin film on Al_2O_3 (0001) substrate is presented in Fig. 4(a), which exhibits a sharp interface without amorphous or microcrystalline layers. Besides, EDS mappings of Ni, Al and O elements also verify the sharp interface without Ni diffusion into Al_2O_3 substrate (see Fig. S2 in the supporting information). Fig. 4(b) and (c) show the fast Fourier transform (FFT) patterns obtained from NiO and Al_2O_3 layers, respectively. These two diffraction patterns, as well as the one attained from the interface area (see Fig. S3 in the supporting information), confirm the epitaxial growth. Some additional diffraction spots have been observed in NiO layer, as shown in Fig. 4(b). Two single crystal domains, where one is rotated by 60^o with reference to the other around [111] axis, are thought to be responsible for such additional diffraction spots [32].

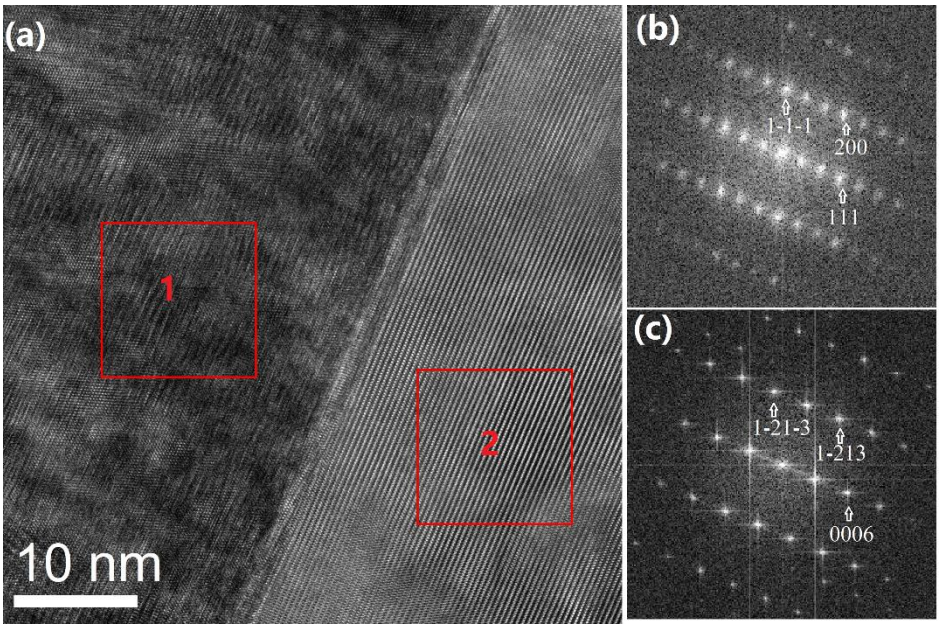

Fig. 4 (a) HRTEM image of epitaxial NiO thin film on Al_2O_3 (0001) substrate. (b) and (c) are the FFT patterns of selected regions marked as 1 and 2 in (a), respectively, corresponding to NiO and Al_2O_3 layers.

3.3. Tuning the optical transmittance

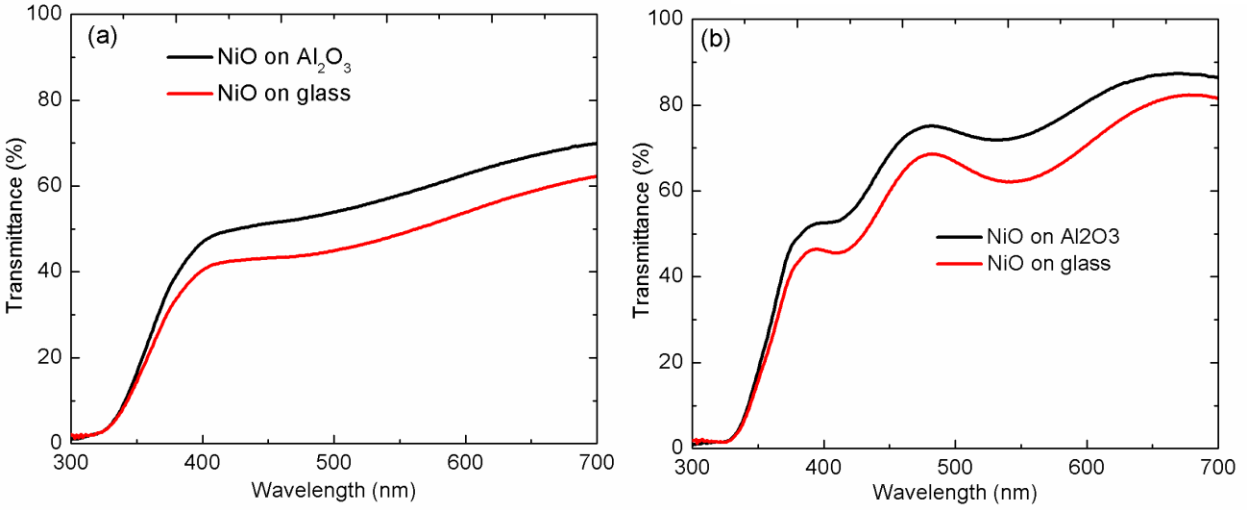

Fig. 5 Optical transmittance of NiO thin films grown on glass and single crystal Al_2O_3 (0001) substrates with different deposition conditions. (a) Oxygen flow rate of 11 sccm and total

sputtering pressure of 0.5 Pa. (b) Oxygen flow rate of 6 sccm and total sputtering pressure of 1 Pa.

The influence of various textures on the optical properties of NiO thin films has been investigated. Fig. 5(a) shows the optical transmittance of NiO thin films on glass and Al_2O_3 (0001) substrates with random and in-plane textures, respectively. Texture affects the optical transmittance, as the transmittance in the whole wavelength range of epitaxial NiO thin film is higher than that of the randomly textured film deposited at the same time. However, the optical band gap of NiO thin films is less sensitive to texture, as the epitaxial and random textured NiO thin films exhibit almost the same absorption edges (corresponding to the optical bang gap of 3.53 eV, as shown in Fig. S4 in the supporting information). Similar situations are observed in fiber textured NiO thin films deposited with the total sputtering pressure of 1 Pa, as shown in Fig. 5(b). Due to the different thickness of NiO thin films deposited with 3, 5 and 6 sccm O_2, it is non-sense to compare their absolute transmittance directly. However, the transmittance discrepancy between films on glass and Al_2O_3 (0001) substrates can provide reliable information. The average transmittance in the visible range (390−700 nm) of films on Al_2O_3 (0001) (T_a), on glass (T_g), as well as their difference ($\Delta T = T_a - T_g$), are summarized in Table I. Interestingly, it is shown that poorer self-texture is beneficial to the enhancement of optical transmittance of film on Al_2O_3 (0001). For instance, ΔT between epitaxial and random textured thin films is as high as 8.4 %. But in the case of NiO thin films deposited with the oxygen flow rate of 3 sccm at the total pressure of 1 Pa, the strong <100> self-texture (see Fig. 2(b)) just gives the ΔT of 3.3 %. This can be qualitatively understood from the grain boundaries related refraction. As seen in Fig. 2(b) and (d), once the orientation of strong self-texture differs with that from the substrate, the competition may yield the poor texture for thin films on matched substrates. Consequently, much more grain boundaries with various orientations may exist in the thin films, which will generally reduce the transmittance due to the increasing refraction at the grain boundaries [15,33]. These results demonstrate that self-texture can also be used to tune the optical transmittance when depositing thin films on matched substrates.

Table I Average transmittance of NiO thin films on Al_2O_3 (0001) (T_a), on glass (T_g), and their difference ($\Delta T = T_a - T_g$) with various deposition conditions.

Deposition conditions	T_g (%)	T_a(%)	ΔT (%)
O_2 flow rate: 11 sccm	49.8	58.2	8.4
Total pressure: 0.5 Pa			
O_2 flow rate: 6 sccm	66.6	74.6	8
Total pressure: 1 Pa			
O_2 flow rate: 5 sccm	67.4	73.7	6.3
Total pressure: 1 Pa			
O_2 flow rate: 3 sccm	57.5	60.8	3.3
Total pressure: 1 Pa			

4. **Conclusions**

NiO thin films with random, fiber and in-plane textures have been successfully deposited at room temperature by reactive magnetron sputtering on glass, silicon and Al_2O_3 (0001) substrates. Comparing the textures of NiO thin films on non-matched amorphous and matched single crystal substrates, it is found that there is strong competition between the driving force from the matched substrate and self-texture. This competition eventually rearranges the orientation and microstructure of thin films on matched substrates. Therefore, tuning this competition is an effective approach to control the texture of thin films on matched substrates. Microstructure analyses at the film/substrate interface region evidence the existence of a nanocomposite layer at the initial growth when depositing thin films on amorphous substrates, where nanocrystals embedded into amorphous matrix. On the contrary, sharp interface without nanocrystals or amorphous layers is observed in in-plane textured NiO thin films on Al_2O_3 (0001) substrates. Besides, it is found that the optical transmittance of NiO thin films on matched substrates can also be tuned by the competition between self-texture and driving force from the matched substrate.

Acknowledgments

Y. Wang is grateful for funding support by the National Natural Science Foundation of China (51702267) and the funding of Southwest University of Science and Technology (16zx7165).

References

[1] C. Detavernier, A.S. Ozcan, J. Jordan-Sweet, E.A. Stach, J. Tersoff, F.M. Ross, C. Lavoie, An off-normal fibre-like texture in thin films on single-crystal substrates, Nature. 426 (2003) 641–645. doi:10.1038/nature02176.1.

[2] N. Fujimura, T. Nishihara, S. Goto, J. Xu, T. Ito, Control of preferred orientation for ZnO_x films: control of self-texture, J. Cryst. Growth. 130 (1993) 269–279. doi:10.1016/0022-0248(93)90861-P.

[3] G.W. Yan, L. Yu, Y. Wang, H. Zhang, P.X. Zhang, H.U. Habermeier, Thermoelectric conversion via laser-induced voltage in highly textured polycrystalline Na_xCoO_2 ceramic, J. Appl. Phys. 110 (2011) 103102. doi:10.1063/1.3660781.

[4] B. Pecquenard, F. Le Cras, D. Poinot, O. Sicardy, J.P. Manaud, Thorough characterization of sputtered CuO thin films used as conversion material electrodes for lithium batteries, ACS Appl. Mater. Interfaces. 6 (2014) 3413–3420. doi:10.1021/am4055386.

[5] I. Petrov, P.B. Barna, L. Hultman, J.E. Greene, Microstructural evolution during film growth, J. Vac. Sci. Technol. A. 21 (2003) S117. doi:10.1116/1.1601610.

[6] S. Vepřek, The search for novel, superhard materials, J. Vac. Sci. Technol. A. 17 (1999) 2401. doi:10.1116/1.581977.

[7] Y. Wang, J. Ghanbaja, S. Bruyère, P. Boulet, F. Soldera, D. Horwat, F. Mücklich, Local heteroepitaxial growth to promote the selective growth orientation, crystallization and

interband transition of sputtered NiO thin films, CrystEngComm. 18 (2016) 1732–1739. doi:10.1039/C5CE02419F.

[8] Y. Wang, J. Ghanbaja, F. Soldera, P. Boulet, D. Horwat, F. Mücklich, J.F. Pierson, Controlling the preferred orientation in sputter-deposited Cu_2O thin films: Influence of the initial growth stage and homoepitaxial growth mechanism, Acta Mater. 76 (2014) 207–212. doi:10.1016/j.actamat.2014.05.008.

[9] A.E. Giba, P. Pigeat, S. Bruyère, T. Easwarakhanthan, F. Mücklich, D. Horwat, Controlling refractive index in AlN films by texture and crystallinity manipulation, Thin Solid Films. 636 (2017) 537–545. doi:10.1016/j.tsf.2017.06.057.

[10] W. Chamorro, D. Horwat, P. Pigeat, P. Miska, S. Migot, F. Soldera, P. Boulet, F. Mücklich, Near-room temperature single-domain epitaxy of reactively sputtered ZnO films, J. Phys. D. Appl. Phys. 46 (2013) 235107. doi:10.1088/0022-3727/46/23/235107.

[11] S. Suwas, N.P. Gurao, Texture Evolution in Thin Films, in: Crystallogr. Texture Mater. Eng. Mater. Process., Springer-Verlag London, 2014. doi:10.1007/978-1-4471-6314-5.

[12] Y. Wang, J. Ghanbaja, F. Soldera, S. Migot, P. Boulet, D. Horwat, F. Mücklich, J.F. Pierson, Tuning the structure and preferred orientation in reactively sputtered copper oxide thin films, Appl. Surf. Sci. 335 (2015) 85–91. doi:10.1016/j.apsusc.2015.02.028.

[13] L. Yu, L. Gu, Y. Wang, P.X. Zhang, H.U. Habermeier, Epitaxial layered cobaltite Na_xCoO_2 thin films grown on planar and vicinal cut substrates, J. Cryst. Growth. 328 (2011) 34–38. doi:10.1016/j.jcrysgro.2011.06.033.

[14] Y. Wang, L. Yu, B. Jiang, P.X. Zhang, Transverse thermoelectric response in tilted orientation $La_{1-x}Sr_xCoO_3$ ($0.05 \leq x \leq 0.4$) thin films, J. Appl. Phys. 110 (2011) 123111. doi:10.1063/1.3673552.

[15] Y. Wang, P. Miska, D. Pilloud, D. Horwat, F. Mücklich, J.F. Pierson, Transmittance enhancement and optical band gap widening of Cu_2O thin films after air annealing, J. Appl. Phys. 115 (2014) 073505. doi:10.1063/1.4865957.

[16] F. Ying, R.W. Smith, D.J. Srolovitz, The mechanism of texture formation during film growth: The roles of preferential sputtering and shadowing, Appl. Phys. Lett. 69 (1996)

3007–3009. doi:10.1063/1.116821.

[17] J.E. Greene, J.E. Sundgren, L. Hultman, I. Petrov, D.B. Bergstrom, Development of preferred orientation in polycrystalline TiN layers grown by ultrahigh vacuum reactive magnetron sputtering, Appl. Phys. Lett. 67 (1995) 2928. doi:10.1063/1.114845.

[18] M.D. Irwin, J.D. Servaites, D.B. Buchholz, B.J. Leever, J. Liu, J.D. Emery, M. Zhang, J.H. Song, M.F. Durstock, A.J. Freeman, M.J. Bedzyk, M.C. Hersam, R.P.H. Chang, M.A. Ratner, T.J. Marks, Structural and electrical functionality of NiO interfacial films in bulk heterojunction organic solar cells, Chem. Mater. 23 (2011) 2218–2226. doi:10.1021/cm200229e.

[19] W.Z. Chang, J.P. Chu, S.F. Wang, Resistive switching behavior of a thin amorphous rare-earth scandate: Effects of oxygen content, Appl. Phys. Lett. 101 (2012) 012102. doi:10.1063/1.4732079.

[20] D.S. Jeong, R. Thomas, R.S. Katiyar, J.F. Scott, H. Kohlstedt, A. Petraru, C.S. Hwang, Emerging memories: Resistive switching mechanisms and current status, Reports Prog. Phys. 75 (2012). doi:10.1088/0034-4885/75/7/076502.

[21] T. Dutta, P. Gupta, A. Gupta, J. Narayan, Effect of Li doping in NiO thin films on its transparent and conducting properties and its application in heteroepitaxial p-n junctions, J. Appl. Phys. 108 (2010) 1–7. doi:10.1063/1.3499276.

[22] Y.B. Wang, X.H. Wei, L. Chang, D.G. Xu, B. Dai, J.F. Pierson, Y. Wang, Room temperature fabrication of transparent p-NiO/n-ZnO junctions with tunable electrical properties, Vacuum. 149 (2018) 331–335. doi:10.1016/j.vacuum.2018.01.015.

[23] M. Jones, I.. McColl, D.. Grant, Effect of substrate preparation and deposition conditions on the preferred orientation of TiN coatings deposited by RF reactive sputtering, Surf. Coatings Technol. 132 (2000) 143–151. doi:10.1016/S0257-8972(00)00867-7.

[24] T. Shinagawa, Y. Ida, K. Mizuno, S. Watase, M. Watanabe, M. Inaba, A. Tasaka, M. Izaki, Controllable Growth Orientation of Ag_2O and Cu_2O Films by Electrocrystallization from Aqueous Solutions, Cryst. Growth Des. 13 (2013) 52–58. doi:10.1021/cg300813z.

[25] K. Martin, G. McCarthy, North Dakota State Univ., Fargo, ND, USA., ICDD Grant-in-

Aid (1991), n.d.

[26] J.H. Lee, Y.H. Kwon, B.H. Kong, J.Y. Lee, H.K. Cho, Biepitaxial growth of high-quality semiconducting NiO thin films on (0001) Al_2O_3 substrates: Microstructural characterization and electrical properties, Cryst. Growth Des. 12 (2012) 2495–2500. doi:10.1021/cg3001174.

[27] R. Yamauchi, Y. Hamasaki, T. Shibuya, A. Saito, N. Tsuchimine, K. Koyama, A. Matsuda, M. Yoshimoto, Layer matching epitaxy of NiO thin films on atomically stepped sapphire (0001) substrates, Sci. Rep. 5 (2015) 14385. doi:10.1038/srep14385

[28] P. Zhai, Q. Yi, J. Jian, H. Wang, P. Song, C. Dong, X. Lu, Y. Sun, J. Zhao, X. Dai, Y. Lou, Hao Yang, G. Zou, Transparent p-type epitaxial thin films of nickel oxide, Chem. Comm. 50 (2014) 1854-1856. doi:10.1039/c3cc48877b

[29] E. Lindahl, J. Lu, M. Ottosson, J.-O. Carlsson, Epitaxial NiO (1 0 0) and NiO (1 1 1) films grown by atomic layer deposition, J. Cryst. Growth, 311 (2009) 4082-4088. doi: 10.1016/j.jcrysgro.2009.06.030

[30] R. Chaim, O.R. Bar-Hama, Densification of nanocrystalline NiO ceramics by spark plasma sintering, Mater. Sci. Eng. A. 527 (2010) 462–468. doi:10.1016/j.msea.2009.10.011.

[31] S. Mahieu, D. Depla, Correlation between electron and negative O- ion emission during reactive sputtering of oxides, Appl. Phys. Lett. 90 (2007) 121117. doi:10.1063/1.2715113.

[32] K. Uchida, K.I. Yoshida, D. Zhang, A. Koizumi, S. Nozaki, High-quality single crystalline NiO with twin phases grown on sapphire substrate by metalorganic vapor phase epitaxy, AIP Adv. 2 (2012) 2–7. doi:10.1063/1.4769082.

[33] R. Apetz, M.P.B. van Bruggen, Transparent Alumina: A Light-Scattering Model, J. Am. Ceram. Soc. 86 (2003) 480–486. doi:10.1111/j.1151-2916.2003.tb03325.x.